Dynamical simulation for long-time relaxation from metastable states: quantitative estimation of coercive field and relaxation time

Masamichi Nishino[1,*] and Seiji Miyashita[2,3]

[1] *Research Center for Materials Nanoarchitectonics, National Institute for Materials Science, 1-1 Namiki, Tsukuba, Ibaraki 305-0044, Japan*

[2] *JSR-UTokyo Collaboration Hub, CURIE, Department of Physics, The University of Tokyo, 7-3-1 Hongo, Tokyo 113-0033, Japan*

[3] *The Physical Society of Japan, 2-31-22 Yushima, Tokyo 113-0033, Japan*

(Dated: October 26, 2024)

The bistability of spin-transition materials is the origin of their multifunctional properties. It causes hysteresis phenomena, i.e., relaxation from a metastable state, of the spin (electronic) state, magnetization, etc. The collapse of a strong metastable state is a long-time relaxation phenomenon. To study such nonequilibrium dynamical phenomenon, time evolution dynamics analyses are important. However, it is difficult to estimate long-time relaxation phenomena by studying time evolution dynamics simulations due to the limitation of the simulation time. Furthermore, because the relaxation occurs in a stochastic process, a wide distribution of the relaxation time has to be considered in the analysis of the relaxation. To overcome these difficulties, we recently developed two methods for the quantitative estimation of the relaxation time from a metastable magnetic state and of the coercive field. In the first method, the relaxation time and coercive field are estimated using the survival (unrelaxed) probability of the ensemble of systems at each field, which extends the limitation of the simulation time. In the second method, they are estimated from the field-dependent free energy barrier obtained from the survival probability under a sweeping field. These methods are applicable to the estimation of the relaxation time and coercive field of any magnetic particles. In this paper, staring with the Stoner-Wohlfarth model, the difference in the characteristic features of the magnetization reversal dynamics between zero and finite temperatures is discussed. Then, the methods of quantitative estimation of the coercive field and relaxation time are presented. The estimation of them using a neodymium permanent magnet grain was demonstrated with the two methods, and the methodological features and the validity of the estimation were discussed. The present study has a common theme to general metastable states including spin transitions.

I. INTRODUCTION

Spin-transition (ST) materials such as spin-crossover compounds [1, 2], Prussian blue analogues [3, 4], etc. have potential as multifunctional materials that can be applied to molecular information storage media, sensors, and actuators. The bistability of the spin (electronic) state of the ST materials causes thermal hysteresis, Light-Induced Excited Spin State Trapping (LIESST), photoinduced switching, etc. [1–4].

The bistability due to a magnetic anisotropy leads to magnetization (magnetic order) hysteresis and coercivity [5–8]. Recently, the coercivity control by using nanoparticles based on molecular magnet materials and metal oxides have been investigated. Such nanoparticles have potential to control the coercive field (force) in microscopic space. For example, in core-shell and core-multishell nanoparticles of Prussian blue analogues, a variation of the coercive field by using different shells has been shown [5], and in nanoparticles of epsilon iron oxide (ε-Fe_2O_3), huge coercive fields have been demonstrated [7, 8]. To understand such hysteresis phenomena, it is important to study the relaxation process from metastable states [9]. In the present work, we study the relaxation process from magnetic metastable states.

The Stoner-Wohlfarth (SW) model [10] describes well the magnetization reversal and coercive field of a magnetic particle (grain) at zero temperature. However, the coercive field at finite temperatures shows a large reduction from the SW field [11]. With increasing the reversed magnetic field, the (free) energy shape changes from Fig. 1(a) to Fig. 1(c). At zero temperature, magnetization reversal occurs deterministically at the threshold field depiced in Fig. 1(b).

At finite temperatures, however, a barrier crossing dynamics (Fig. 1(a)) becomes essential and the treatment of the thermal effects is important in theoretical investigations of the coercivity. Coercive field H_c is caused by a hysteresis nature of magnets, i.e., a nonequilibrium dynamical phenomenon with a long-time relaxation process. Thus, time evolution dynamics analyses are important to approach the mechanism of coercivity. However, there exists a difficulty in time evolution dynamics simulations, i.e., simulation time. In experiments of permanent magnets, a coercive field is often defined as a field in which the metastable magnetic state has a lifetime of 1 s, the relaxation time of 1 s. On the other hand, a practical simulation time of real time dynamics using equations of motion is around 1 ns, and it is too short to study such a long-time relaxation process. Simulation time is a common problem for studies of long-time relaxation phenomena in all real systems, e.g., protein folding.

* Corresponding author: nishino.masamichi@nims.go.jp

We review our recent works to study the relaxation time of metastable states and the estimation of coercivity. The studies have been performed for a ferromagnetic grain [12, 13], but they have a common theme to general metastable states including spin transitions. To begin with, the characteristics of the SW model are explained. Then, we show that the dynamical features of magnetic grains with metastable states at zero temperature are well described by the SW model. Next, we study the coercive field of the grain at finite temperatures and discuss the difference in dynamics between zero and finite temperatures.

We show two methods to quantitatively estimate the coercive field and relaxation time of a magnetic grain. We demonstrate estimations of the coercive field of a grain of the Nd permanent magnet ($Nd_2Fe_{14}B$ [14–24]), known a strong magnet, as an example. The first one is a method to extend the limitation of simulation time [12]. In this method, first, a simulation of magnetization reversal for many samples in a time period ($t < 1$ ns) is performed under a fixed field, and the survival (unrelaxed) probability as a function of time (t) is observed. Then, using a statistical relation to the probability, a much longer life time (relaxation time) up to microseconds or submicroseconds is estimated. Finally, the field for the 1 s relaxation time is estimated by an extrapolation of the relaxation time as a function of the field. Because the relaxation time increases very rapidly in the field region approaching the coercive field, the obtained coercive field is a good estimation.

The second method evaluates a coercive field and relaxation time by estimating the free energy barrier using a magnetic field sweep [13]. In this method, a simulation of magnetization reversal is performed for many samples under a sweeping field, and the survival (unrelaxed) probability is observed as a function of the field. From this probability, the free energy barrier is estimated, and the coercive field is obtained from an analysis of the field-dependent barrier. We show the agreement of the estimated coercive force between the two methods. In this method, not only coercive field but also zero-field energy barrier and field for zero-energy barrier can be estimated. The estimation of a coercive field from an analysis of the free-energy barrier as a function of magnetization can be performed using a Monte Carlo simulation [25] with the Wang-Landau algorithm [26]. However, the MC method requires very heavy computational cost with complexity as well as the first method, and the second method is a more convenient one to obtain a coercive field. These methods are applicable to any magnetic particles such as molecular magnets and metal oxide.

The rest of the paper is organized as follows. In Sec. II A, the characteristics of a SW particle are shown. In Secs. II B and II C, the dynamical features of magnetization reversal of a grain at zero temperature and at finite temperatures are described, respectively. In Sec. III A, the first method for estimating the coercive field and relaxation time is presented using an example of a grain of the Nd permanent magnet. In Sec. III B, the second method for estimating the coercive field and relaxation time is demonstrated. The validity of this method is discussed in comparison to the first method. Section IV is devoted to the summary. In Appendix A, the details of the atomistic model of the Nd magnet is given.

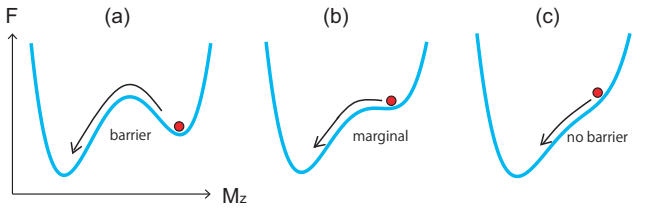

FIG. 1. Typical free-energy barrier types for magnetization reversal. (a) Barrier crossing type, (b) marginal type, and (c) no-barrier type. Types (a), (b), and (c) cause stochastic, intermediate, and deterministic dynamics, respectively.

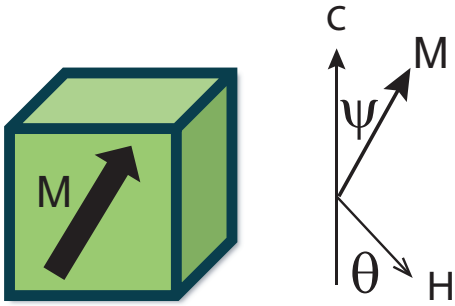

FIG. 2. Stoner-Wohlfarth particle. ψ is the angle between the c axis (easy axis) and magnetization (M) and θ between the negative c direction and magnetic field (H).

II. MAGNETIZATION REVERSAL AT ZERO AND FINITE TEMPERATURES

A. Stoner-Wohlfarth model

First, we show the SW threshold field of a uniaxial single particle with the anisotropy constant K and magnetization M (Fig. 2). Under a reversed field H, the energy of the single particle is given as

$$E = K\sin^2\psi - MH\cos(\pi - \psi - \theta). \qquad (1)$$

Here, ψ is the angle between the c axis (easy axis) and magnetization (M) and θ between the negative c direction and magnetic field (H).

The instability condition for the magnetization reversal is given by the relations:

$$\frac{\partial E}{\partial \psi} = K\sin 2\psi - MH\sin(\pi - \psi - \theta) = 0 \qquad (2)$$

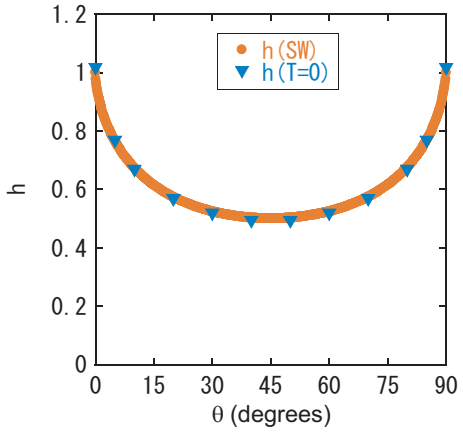

FIG. 3. θ dependence of the threshold field h_c of the Stoner-Wohlfarth grain and comparison with that of the Heisenberg model with the anisotropy at zero temperature $T = 0$.

and

$$\frac{\partial^2 E}{\partial \psi^2} = 2K\cos 2\psi + MH\cos(\pi - \psi - \theta) = 0. \quad (3)$$

The θ dependence of the threshold field is derived from these equations as

$$h_c = \frac{H}{H_{SW}} = \frac{1}{\cos\theta\{1 + (\tan\theta)^{2/3}\}^{3/2}}, \quad (4)$$

where the the SW field at $\theta = 0$, i.e.,

$$H_{SW} \equiv \frac{2K}{M}, \quad (5)$$

is taken as the unit for the external field. The critical angle of the spin is given as

$$\psi_c = \tan^{-1}\sqrt[3]{\tan\theta}. \quad (6)$$

The θ dependence of h_c is depicted in Fig. 3. The threshold filed h_c is found to be symmetric regarding $\theta = 45°$.

B. Uniform rotation of magnetization at zero temperature

Next, we show the feature of magnetization reversal in a single grain described by the Heisenberg Hamiltonian with a magnetocrystalline anisotropy:

$$\mathcal{H} = -\sum_{\langle i,j\rangle} J_{i,j}\boldsymbol{S}_i \cdot \boldsymbol{S}_j - \sum_{i=1}^{N} D_i (S_{i,z})^2 - \sum_{i=1}^{N} \boldsymbol{H}\cdot\boldsymbol{S}_i. \quad (7)$$

Here, $\boldsymbol{S}_i$ is the ith spin (magnetic moment) and $J_{i,j}$ is the exchange interaction between the ith and jth sites which are a nearest-neighbor pair denoted by $\langle i,j\rangle$. D_i is the magnetic anisotropy constant at the ith site, H is the magnetic field, and N is the number of spins.

We studied a cubic single grain of 10^3 sites (Fig. 2). The exchange interaction energy is usually larger than the anisotropy energy and the parameters of the model were set to $J_{i,j} = 1.0$, $D_i = 0.2$, and $S_i = 1.0$ as an example case. Other choices such as $D = 0.1$ and $S = 2.0$, $D = 0.3$ and $S = 2.5$, etc. do not change the contents and arguments of the paper. The critical temperature of the model (7) for $D_i = 0$ and $H = 0$ is $T_c = 1.443J$ [27]. The critical temperature for $D_i = 0.2$ is slightly higher but very close to T_c. There is no thermal fluctuation at zero temperature, $T = 0$, and the threshold field corresponds to the field at which the energy barrier vanishes. It corresponds to Fig. 1(b). In this case, magnetization reversal occurs in a deterministic process.

1. *Landau-Lifshitz-Gilbert equation*

The threshold field for magnetization reversal is obtained by studying the Landau-Lifshitz-Gilbert (LLG) equation. As long as the field is weaker than the threshold value, no reversal occurs in a LLG simulation but a reversal occurs in a short time at the threshold field. The time-evolution of the ith spin in the system is given as

$$\frac{d}{dt}\boldsymbol{S}_i = -\frac{\gamma}{1+\alpha_i^2}\boldsymbol{S}_i \times \boldsymbol{H}^{\rm eff} - \frac{\alpha_i\gamma}{(1+\alpha_i^2)S_i}\boldsymbol{S}_i \times [\boldsymbol{S}_i \times \boldsymbol{H}^{\rm eff}]. \quad (8)$$

Here, the parameter γ is the electron gyromagnetic ratio and α_i is the damping parameter. The effective field $\boldsymbol{H}^{\rm eff}$ is given by

$$\boldsymbol{H}^{\rm eff} = -\frac{\partial \mathcal{H}}{\partial \boldsymbol{S}_i}. \quad (9)$$

2. *Threshold field at zero temperature*

The threshold field $h_c(\theta)$ at $T = 0$ are plotted by bule inverted triangles in Fig. 3, where

$$H_{SW} \equiv 2D/S. \quad (10)$$

The simulation data at $T = 0$ agreed with the SW curve. Figure 4 shows snapshots in magnetization reversal at $T = 0$ at the threshold field for $\theta = 0$. The reversal occured in a uniform rotation, in which $J_{i,j}$ was not important. h_c agreed with Eq. (4) with $H_{SW} \equiv 2D/S$. The reversal dynamics at zero temperature is described well by the SW dynamics.

C. Magnetization reversal with nucleation at finite temperatures

In contrast to the zero temperature case, the nucleation mechanism is important for magnetization reversal at finite temperatures, where thermal fluctuation plays an significant role. In this case, magnetization reversal

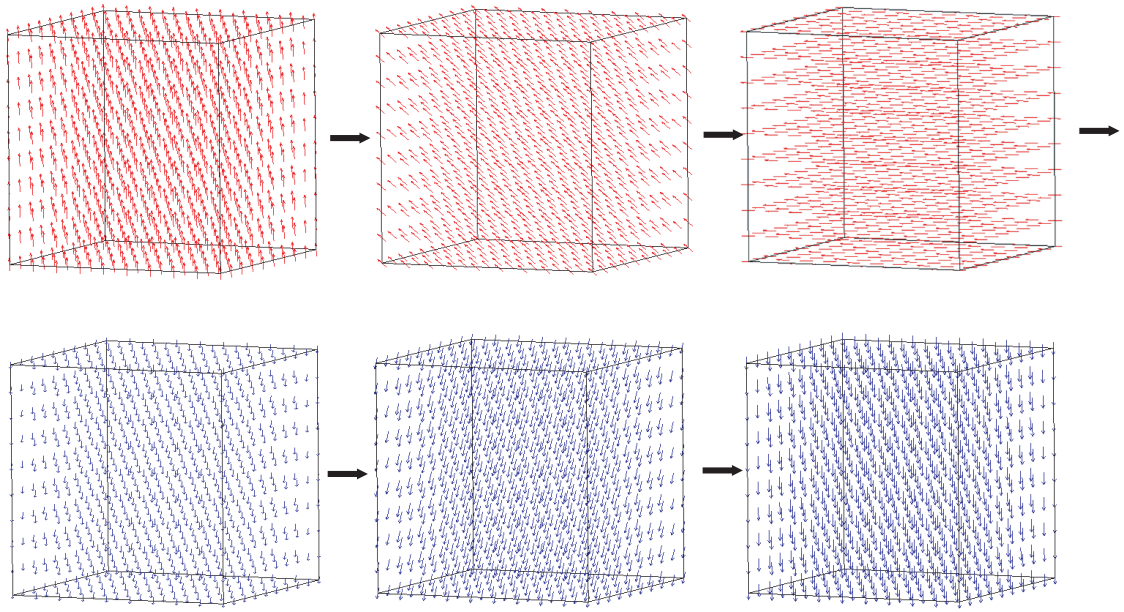

FIG. 4. Snapshots of magnetization reversal at the threshold field at zero temperature ($T = 0$) in model (7). Red and blue arrows denote up and down spins, respectively. Uniform rotation is observed.

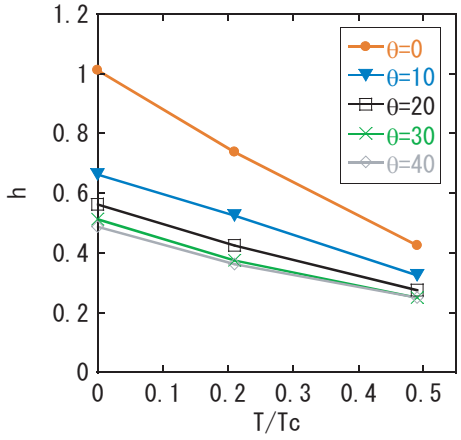

FIG. 5. Temperature dependence of the threshold field (h_c) at several angles θ (°) of the magnetic field in model (7).

occurs stochastically because a stochastic jump over the barrier occurs by thermal fluctuation (Fig. 1(a)).

1. *Stochastic Landau-Lifshitz-Gilbert equation*

To treat the thermal fluctuation, a noise field is introduced into the effective field $\boldsymbol{h}_i^{\rm eff}$ on the ith spin as

$$\boldsymbol{H}^{\rm eff} = -\frac{\partial \mathcal{H}}{\partial \boldsymbol{S}_i} + \boldsymbol{\xi}_i(t). \tag{11}$$

Here, $\boldsymbol{\xi}_i(t) = (\xi_i^x, \xi_i^y, \xi_i^z)$ is a white Gaussian noise, which satisfies the following relations:

$$\langle \xi_i^\mu(t) \rangle = 0, \quad \langle \xi_i^\mu(t) \xi_j^\nu(s) \rangle = 2\mathcal{D}\delta_{ij}\delta_{\mu\nu}\delta(t-s). \tag{12}$$

Here, $\mathcal{D}_i$ is the amplitude of the noise. When the relation:

$$\mathcal{D}_i = \frac{\alpha_i k_{\rm B} T}{\gamma S_i} \tag{13}$$

is satisfied, the system relaxes to a steady state (equilibrium) in the canonical distribution at temperature T. The LLG equation (Eq. (8)) with the effective field including the noise is called the stochastic Landau-Lifshitz-Gilbert (sLLG) equation [28, 29].

2. *Threshold field at finite temperatures*

Simulations were carried out by solving the sLLG equation numerically in Stratonovich interpretation. We used a kind of middle point method equivalent to the Heun method for the numerical integration [29]. α_i was set to 0.1. We observed the magnetization reversal within 1×10^6 updates ($t = 10^4$) with time steps of $\Delta t = 0.01$ at each magnetic field. In the present notation, the period of the precession is of order O(1), and $\Delta t = 0.01$ is small enough to simulate the situation. The coercive field is experimentally estimated in a 1s observation, which corresponds to a simulation time of order $t \sim 10^{12}$, and it is much longer than the simulation time. However, the relaxation time becomes longer exponentially around

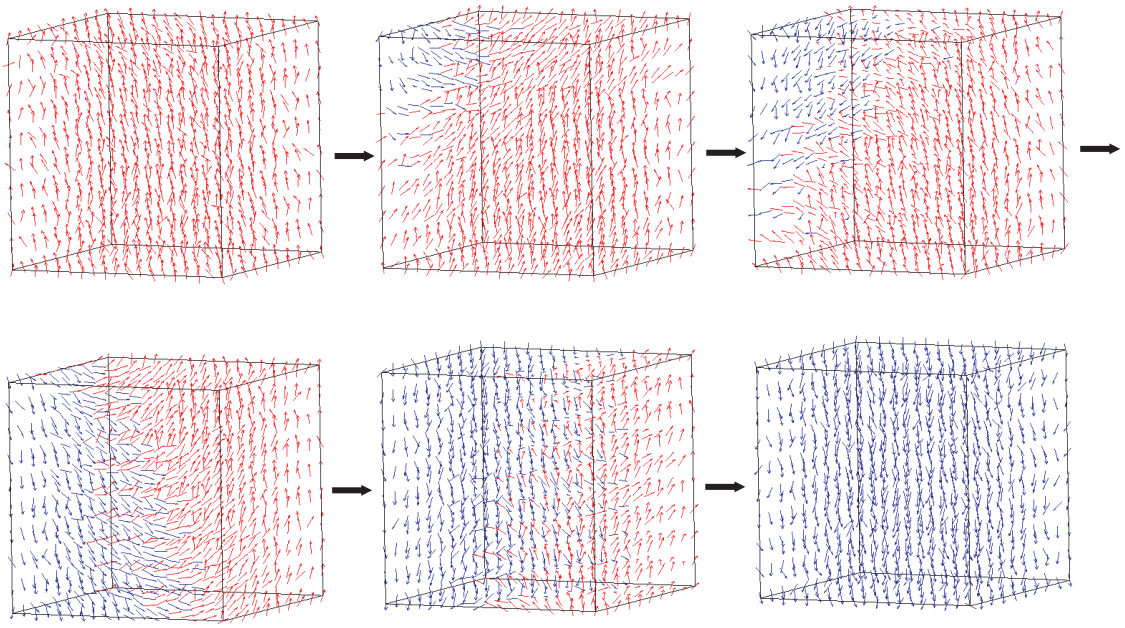

FIG. 6. Snapshots of magnetization reversal at the threshold field at a finite temperature ($T = 0.21T_c$) in model (7). Nucleation is observed.

the threshold field [12, 27], and the threshold fields estimated here are approximation to the coercive fields. We discuss the exponential growth of the relaxation time in Sec. III A.

In Fig. 5, temperature dependence of $h_c(\theta)$ are plotted at several angles θ (°) of the magnetic field in model (7). We found that the thermal fluctuation effect significantly reduces threshold fields, h_c decreases with temperature approximately linearly, and h_c at $\theta = 0$ shows the largest decreases with temperature.

Figure 6 presents snapshots of a reversal at $T = 0.21T_c$ at the threshold field for $\theta = 0$. A local nucleation (in this case, corner) was found. This suggests that the nucleation mechanism is essential for the reversal at finite temperatures. The corner spins have weaker exchange interactions due to fewer neighbors, nucleation occurs easily at the corner with thermal fluctuation.

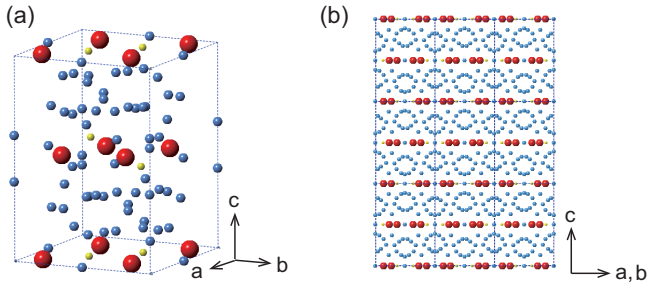

FIG. 7. (a) Unit cell of the Nd magnet. (b) Side view of 3×3 unit cells.

III. ESTIMATION OF COERCIVE FIELD

When the field is relatively weak at finite temperatures, thermal fluctuation causes magnetization reversal stochastically in a barrier crossing process (Fig. 1), and the relaxation time is widely distributed. This situation makes an estimation of coercive field (force) difficult.

In this section, we show how to estimate the coercive field of a grain at finite temperatures using an example of a Nd magnet grain. The unit cell of the magnet and side view of 3×3 unit cells are illustrated in Fig. 7. Fe and Nd atoms are magnetic sites and the location of them is complicated. The methods presented here are applicable to any magnetic materials such as molecular magnets, etc.

A. Estimation using survival probability under a fixed field

1. *Relaxation time*

We observed magnetization reversal of a single grain of $12 \times 12 \times 9$ unit cells (10.56 nm × 10.56 nm × 10.971 nm) of the Nd magnet by the sLLG method under a fixed reversed field parallel to the easy axis ($\theta = 0$) at 0.46 T_c, close to room temperature. The details of the Hamiltonian of the Nd magnet is given in appendix A. Here, $\Delta t = 0.1$ fs was used. If the reversed magnetic field

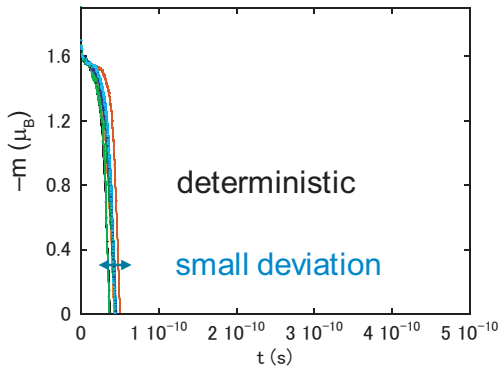

FIG. 8. Samples of time dependence of magnetization at $H = 8$ T. $\alpha_i = 0.1$. Deterministic reversal.

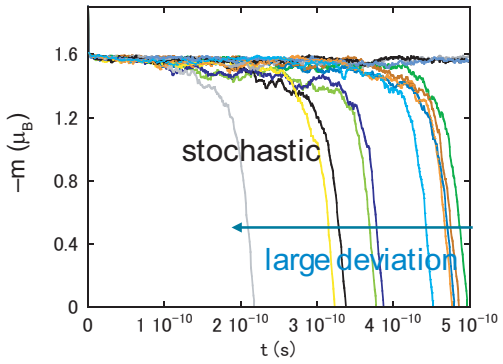

FIG. 9. Samples of time dependence of magnetization at $H = 4.1$ T. $\alpha_i = 0.1$. Stochastic reversal.

is strong, the relaxation (magnetization reversal) occurs in a deterministic process, while if the field is weak, the relaxation is a stochastic process. We measured the per-site magnetization:

$$m = \frac{1}{N_{\rm site}} \sum_{i=1}^{N_{\rm site}} S_i^z, \tag{14}$$

where $N_{\rm site}$ is the number of the atoms (magnetic sites) in the system.

Samples of time dependence of magnetization m at $H = 8$ T and $H = 4.1$ T are depicted in Figs. 8 and 9, respectively. Magnetization relaxation curves at $H = 8$ T are deviated in a narrow region. This indicates that the relaxation occurs deterministically and the feature of the free energy as a function of the magnetization corresponds to Fig. 1 (c).

On the other hand, relaxation curves at $H = 4.1$ T are widely deviated and thus the relaxation occurs stochastically and the free energy is like Fig. 1 (a). In this case, due to a large distribution of the relaxation time, a practical estimation of the average relaxation time is very difficult. To overcome this difficulty, we employ the following statistical method for the estimation of the reversal time.

If a magnetization reversal occurs with a probability p in a unit time, the probability to have a reversal for the first time in the period $[t, t+\Delta t]$ is $(1-p\Delta t)^{t/\Delta t} p\Delta t = pe^{-pt}\Delta t$. Thus, the mean relaxation time $\langle\tau\rangle$ is given by

$$\langle\tau\rangle = p\int_0^\infty te^{-pt}dt = \frac{1}{p}. \tag{15}$$

The probability $P(t)$ to have the reversal in the period $[0, t]$ is given by

$$P(t) = \int_0^t pe^{-pt'}dt' = 1 - e^{-pt}. \tag{16}$$

The number of the survival (unchanged) samples ($N_{\rm sv}$) is expressed by

$$N_{\rm sv}(t) = N - NP(t) = Ne^{-pt}, \tag{17}$$

where N is the total number of samples. Then, the average relaxation time $\langle\tau\rangle$ can be estimated from the slope of $\ln(N_{\rm sv}(t)/N)$ as a function of time.

2. *Simulation of magnetization reversal at each field*

Using the formula (17) for $N = 864 \sim 2592$ samples, we estimated $\langle\tau\rangle$ for various values of the field. In Fig. 10, we show an example of $\ln(N_{\rm sv}(t)/N)$ for $H = 4.1$ T. A linear dependence was found after $t = 3\times10^{-10}$ s and using this straight part, the relaxation time $\langle\tau\rangle$ was estimated. In the early period a upward-convex curve appears, which indicates that some additional time is needed in the simulation before the process is governed by a nucleation rate. Thus, the present method has a merit to identify the initial transient process which causes a bias in the simple average of the relaxation time.

We obtained $\langle\tau\rangle = 6.71\times10^{-10}$s ($p = 1.491\times10^9$ (1/s)) by making a linear least-square fitting to the straight part (orange line in Fig. 10). In the same manner, $\langle\tau\rangle$ was estimated for various values of the field between 3.7 and 8 T with different values of the damping parameter α_i (Fig. 11). It should be noted that the simulation time is 0.5 ns but the estimated relaxation time is lager than 10^{-7} s. That is, we succeeded to analyze the relaxation time a thousand times longer than the simulation time. We found a sharp increase of the relaxation time in the stochastic region below around 4.2 T regardless of the value of α_i. To obtain the coercive field, whose relaxation time is 1s, these curves of τ vs. H were extrapolated using a double exponential function, i.e., the Arrhenius law with a correction term:

$$\tau(H) = Ae^{-aH} + Be^{-bH} = Ae^{-aH}\left(1 + Ce^{-dH}\right), \tag{18}$$

where $C = B/A$ and $d = b - a$.

In Fig. 10, the fitted curves of Eq. (18) are plotted for different values of α_i. The intersection of the fitted curve for a given α_i and $\tau = 1$ s gives the expected coercive field. The intersections for $\alpha_i = 0.1$, $\alpha_i = 0.15$,

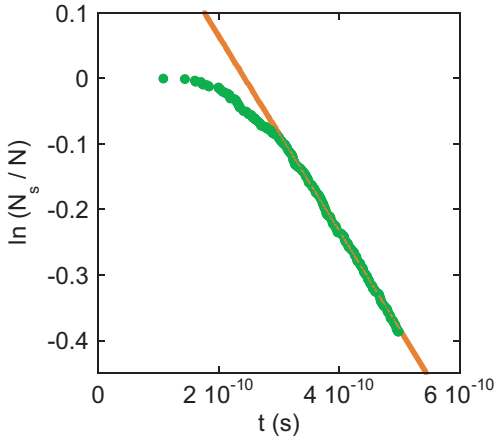

FIG. 10. Time dependence of $\ln(N_s/N)$ at $H = 4.1$T. $\alpha_i = 0.1$.

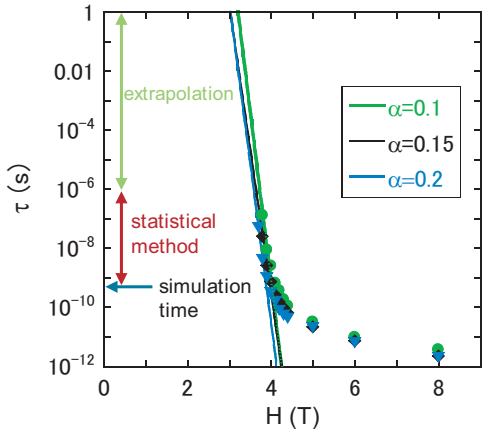

FIG. 11. Field dependence of the magnetization reversal time τ for $\alpha_i = 0.1$ 0.15 and 0.2, and their extrapolations.

and $\alpha_i = 0.2$ are $h_c \simeq 3.2$ T, 3.0 T, and 3.0 T (Av. 3.07 T). Therefore, the coercive fields are found to be around 3 T. We find that, although the simulation time of the dynamical equation is much shorter than 1 s, the statistical method with the extrapolation is effective for the estimation of the coercive force.

B. Estimation using survival probability under field sweep

1. *Survival probability under field sweep*

In this subsection, we show an alternative method to estimate coercive field more conveniently using the field-dependent survival (non-reversal) probability generated by a time evolution simulation under a field sweep.

When the reversed field is relatively weak, a magnetization reversal occurs in a barrier crossing process and the relaxation rate for the stochastic dynamics is given by the Arrhenius rate as

$$R = \frac{1}{\tau_0} e^{-\beta E_{\rm B}(H)}. \tag{19}$$

Here, τ_0 is a pre-exponential factor, which represents of the frequency of the contact with the bath and is of order of the lattice vibration frequency. We adopt a commonly used value for the factor, i.e., $\tau_0 = 10^{-11}$ s [30].

When the reversed field is strong, a magnetization reversal occurs deterministically and the relaxation rate is set to constant:

$$R = const. \tag{20}$$

The relaxation rate should vary with the field even in the deterministic region, but it is much faster than that in the stochastic region, and thus the choice is not relevant to estimate the coercive field.

For an intermediate field, the dynamics has a crossover feature. In this case, an approximate form of relaxation rate can be considered:

$$R = \frac{1}{\tau_0 (e^{\beta E_{\rm B}(H)} + c)}. \tag{21}$$

That is, if $E_{\rm B}(H)$ has a positive large value, corresponding to the stochastic dynamics, $R \simeq \frac{1}{\tau_0} e^{-\beta E_{\rm B}(H)}$, and if $E_{\rm B}(H)$ has a small value, corresponding to the deterministic dynamics, $R \simeq 1/(\tau_0 c)$.

Here, the probability of non-relaxation (avoiding magnetization reversal) is derived when the field is swept until H starting from $H = -\infty$ (all down state). The probability of non-relaxation between t and $t + \Delta t$ is given as $1 - R(H(t))\Delta t = e^{-R(H(t))\Delta t} + O(\Delta t^2)$. Thus the probability of non-relaxation until time t is

$$P(t) = \prod_{m=0}^{n-1} \left[e^{-R(H(t_0 + m\Delta t))\Delta t} \right] + O(\Delta t) \tag{22}$$

$$= \exp\left[-\frac{1}{\tau_0} \int_{-\infty}^{t} \frac{1}{e^{\beta E_{\rm B}(H(t'))} + c} dt' \right]. \tag{23}$$

If the field is swept linearly with time, i.e., $H(t) = vt$, then the probability as a function of H is given as

$$P(H) = \exp\left[-\frac{1}{\tau_0} \int_{H(-\infty)=-\infty}^{H(t)} \frac{1}{e^{\beta E_{\rm B}(h)} + c} \frac{dt}{dh} dh \right]$$

$$= \exp\left[-\frac{1}{v\tau_0} \int_{-\infty}^{H} \frac{1}{e^{\beta E_{\rm B}(h)} + c} dh \right]. \tag{24}$$

We combine this probability with the following formula for the (free) energy barrier:

$$E_{\rm B}(H) = E_0 \left(1 - \frac{H}{H_0} \right)^n. \tag{25}$$

Here, E_0 is the zero-field energy barrier and H_0 is the field for zero-energy barrier. This formula is useful for

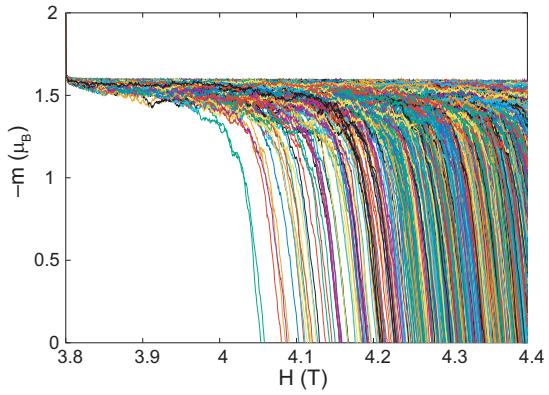

FIG. 12. Magnetization (m) relaxation of many samples as a function of the field in a field sweep with $v = 1.2 \times 10^9$ T/s.

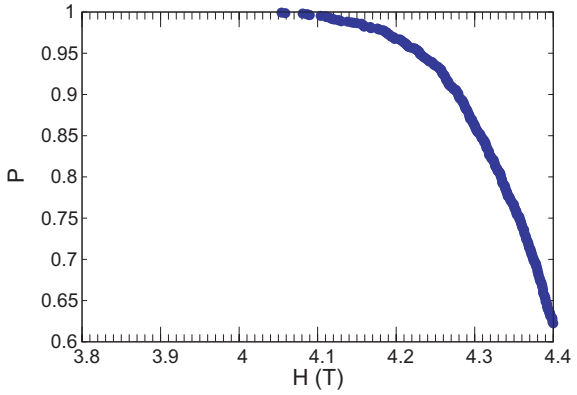

FIG. 13. P(H) in a field sweep with $v = 1.2 \times 10^9$ T/s.

analyses of magnetization reversal in permanent magnets [31–33]. The value of the exponent n is established as $n = 1 \sim 2$ for many magnetic materials. Experiments of several magnets including the Nd magnet supported $n = 1$ [30, 32–37]. We studied the estimation of the coercive field using both $n = 1$ and $n = 2$ in our previous work and found that $= 1$ was valid [13]. Thus, we adopt $n = 1$.

For $E_{\rm B}(H) = E_0\left(1 - \frac{H}{H_0}\right)$, i.e., $n = 1$ case, $P(H)$ is given as

$$P(H) = \exp\left[-\frac{1}{v\tau_0}\int_{-\infty}^{H}\frac{1}{e^{\beta E_0\left(1-\frac{h}{H_0}\right)}+c}dh\right]. \quad (26)$$

This integral can be calculated analytically and the probability is given by

$$P(H) = \exp\left[-\frac{H_0}{cv\tau_0\beta E_0}\ln\left(1+ce^{-\beta E_0(1-\frac{H}{H_0})}\right)\right]. \quad (27)$$

Then we have

$$\ln(-\ln(P(H))) = \ln\left[\frac{H_0}{cv\tau_0\beta E_0}\ln\left(1+ce^{-\beta E_0(1-\frac{H}{H_0})}\right)\right]. \quad (28)$$

In the pure Arrhenius case, i.e, $c \to 0$, the following relation holds.

$$\ln(-\ln P(H)) = \frac{\beta E_0}{H_0}H + \ln\left[e^{-\beta E_0}\frac{H_0}{v\tau_0\beta E_0}\right], \quad (29)$$

which is a linear function of the field H. Therefore, a linear dependence of H for $\ln(-\ln P(H))$ indicates that a stochastic dynamics is realized. On the other hand, when the function of $\ln(-\ln P(H))$ deviates from a linear dependence of H, it suggests that the dynamics is not the stochastic one but intermediate or deterministic one.

Applying the formula (28) or (29) to the field dependence of P obtained by a field sweep simulation using the sLLG method, we can estimate H_0 and βE_0 (optimized values). Once H_0 and βE_0 are obtained, the coercive field, $H_{\rm c}$ is estimated as follows. The relaxation time for the free energy barrier ΔF is given as

$$\begin{aligned}\tau &= \tau_0\exp(\beta\Delta F)\\ &= \tau_0\exp\left(\beta E_0\left(1-\frac{H_{\rm c}}{H_0}\right)\right).\end{aligned} \quad (30)$$

Then, the coercive field is

$$H_{\rm c} = H_0\left(1-\frac{1}{\beta E_0}\ln\frac{\tau}{\tau_0}\right). \quad (31)$$

If the coercive field is defined as the threshold field at which the relaxation time is $1s$, substituting $\tau = 1$ s and $\tau_0 = 10^{-11}$ s into Eq. (31), we have.

$$H_{\rm c} = H_0\left(1-\frac{25.3}{\beta E_0}\right). \quad (32)$$

We used this formula in the present paper. Threshold fields for different relaxation times can also be obtained using Eq. (31). For example, the threshold field at which the relaxation time is 100 s is expressed as $H_{\rm c} = H_0\left(1-\frac{29.9}{\beta E_0}\right)$.

2. *Simulation of magnetization reversal under field sweep*

We performed sLLG simulations to observe magnetization reversal in N samples of an open-boundary system of $12 \times 12 \times 9$ unit cells (10.56 nm $\times$ 10.56 nm $\times$ 10.971 nm) along a, b, and c axes, respectively. The magnetic field is swept with a constant velocity (v) from a low field ($H_{\rm i}$) to a high field ($H_{\rm f}$) and the per-site magnetization m was recorded for each sample. We determined the reversal field as the field when the value of m changes the sign of m. During the field sweeping, the number of the survival (non-relaxed) samples, $N_{\rm s}(H)$, was counted as a function of H. $P(H)$ was estimated as $P(H) = \frac{N_{\rm s}(H)}{N}$.

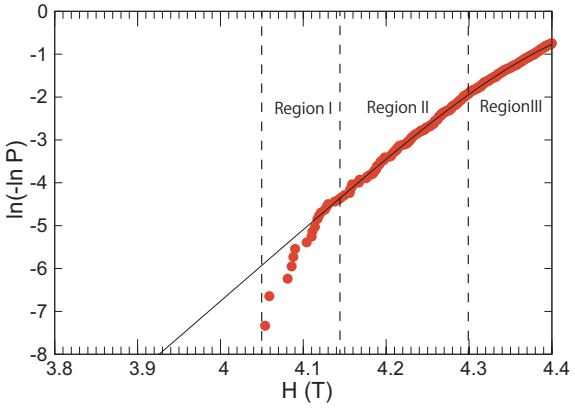

FIG. 14. $\ln(-\ln(P(H)))$ (red circles) under a field sweep at $v = 1.2 \times 10^9$ T/s from $H = 3.8$ T to 4.4 T. Solid curve represents the result of fitting with Eq. (28).

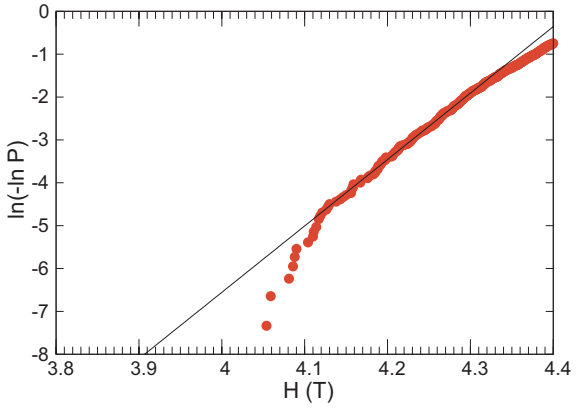

FIG. 15. $\ln(-\ln(P(H)))$ (red circles) under a field sweep at $v = 1.2 \times 10^9$ T/s from $H = 3.8$ T to 4.4 T. Solid line represents the result of fitting with Eq. (29).

We analyzed the data for the sweeping from $H = 3.8$ T to $H = 4.4$ T for 0.5 ns ($v = 1.2 \times 10^9$ T/s). We used different random number sequences for the noise field for $N = 1536$ samples. Magnetization reversal curves (m) and survival probability ($P(H)$) are plotted as a function of the field H in Figs. 12 and 13, respectively. The interval of the reversal field was found to be distributed sparsely at lower fields and the frequency of relaxation increases at higher fields.

In Fig. 14, $\ln(-\ln(P(H)))$ is depicted as a function of H. We found that there are three characteristic regions in the plot.

- Region I: the initial transient region for 4.05 T $\leq H \lessapprox$ 4.15 T.
- Region II: the stochastic relaxation region for 4.15 T $\lessapprox H \lessapprox$ 4.3 T (Fig. 1 (b)). A linear dependence.
- Region III: an intermediate or deterministic region for 4.3 T $\lessapprox H$ (Fig. 1 (c)).

In Region I, the data are located irregularly and deviates from a linear dependence. This indicates the initial transient region, which is a similar situation to the early relaxation in Fig. 10. In Region II, we found a linear dependence, which suggests the stochastic region. Equation (29) holds in this region. In Region III, the plotted data gradually turn and deviate from the straight line, which indicates an intermediate or deterministic region.

We performed a least-square fitting using Eq. (28) with three fitting parameters H_0, βE_0, and c to the data in the region of 4.15 T $\leq H \leq$ 4.4 T. The obtained fitting parameters are given in Table I. We have $H_c \simeq 3.0$ T, $H_0 \simeq 4.5$, and $\beta E_0 \simeq 76$. Even if the region I is included in the fitting, the change of the values of H_c, H_0, and βE_0 are small (Table I).

Then, we estimated H_c, H_0, and βE_0 using Eq. (29) (Fig. 15) and compared them with those using Eq. (28). The obtained fitting parameters are given in Table II. We have $H_c \simeq 2.9$ T, $H_0 \simeq 4.5$, and $\beta E_0 \simeq 70$ and these values are close to those obtained using Eq. (28). Even if other regions are included in the fitting, the change of the values of H_c, H_0, and βE_0 are also small (Table II).

The estimated values of the coercive field here ($H_c \simeq 2.9$–3.0 T) are consistent with those obtained in Sec. III A, i.e., $H_c \simeq 3.0$–3.2 T (Av. 3.07 T) and also consistent with our previous estimation ($H_c \simeq 3.0$–3.1 T) [13]. The estimation of H_c by a free energy analysis using a Monte Carlo study gave a similar value ($H_c \simeq 3.3$T) for the same system [25]. Thus, we concluded that the coercive field of the grain is around 3 T. It is applicable not only to the estimation of H_c but also to those of H_0 and βE conveniently.

TABLE I. Estimated values of H_c, H_0, and βE_0 using Eq. (28) in the fitting range between H_i and H_f for a field sweep at $v = 1.2 \times 10^9$ T/s from $H = 3.8$ T to 4.4 T. The field values are given in Teslas.

$[H_i, H_f]$	H_c	H_0	βE_0	c
[4.15, 4.40]	2.99	4.50	7.55×10^1	1.39×10^1
[4.05, 4.40]	3.14	4.45	8.57×10^1	2.11×10^1

TABLE II. Estimated values of H_c, H_0, and βE_0 using Eq. (29) in the fitting range between H_i and H_f for a field sweep at $v = 1.2 \times 10^9$ T/s from $H = 3.8$ T to 4.4 T. The field values are given in Teslas.

$[H_i, H_f]$	H_c	H_0	βE_0
[4.15, 4.30]	2.90	4.53	7.02×10^1
[4.05, 4.30]	3.04	4.50	7.80×10^1
[4.05, 4.40]	2.86	4.55	6.83×10^1

IV. SUMMARY

The multifunctional properties of spin-transition materials are caused by their bistable nature. The bistabil-

ity leads to hysteresis phenomena, i.e., relaxation from a metastable state, of the spin (electronic) state, magnetization, etc. Thus, time evolution dynamics analyses are important for understanding these nonequilibrium dynamical properties.

In the present paper, we study the relaxation process from magnetic metastable states. To begin with, the properties of the coercivity of the Stoner-Wohlfarth (SW) particle were presented. The zero-temperature characteristics of the coercive field of a magnetic grain were discussed comparing those of the SW particle. The magnetization reversal occurred in uniform rotation at the threshold field, which is essentially the same as the SW particle, and the value of the threshold field coincided that expected from the SW field.

Then, the coercive field and reversal dynamics of the grain at finite temperatures were studied. There, the nucleation mechanism caused by the thermal fluctuation effect played an important role, and it reduced largely the coercive field than the SW field. From the analysis of angle dependence of the coercive field, it was found that when the reversed field is applied in antiparallel to the easy axis (the angle $\theta = 0$), the coercive field was maximum but the reduction rate of the coercivity from that of the zero temperature was also largest.

Next, recent developments in methods of the quantitative estimation of the coercivity and relaxation time of a magnetic grain were demonstrated. The coercivity estimation of a neodymium magnet particle was presented as an example. The focus is on how to overcome the difficulty that the time scale for time evolution dynamics simulations (around ns) is much shorter than the relaxation time for coercivity (1s) and that the relaxation time of a single grain for a magnetization reversal is widely distributed.

First, a method to extend the limitation of simulation time was introduced. In this method, using a statistical relation to the survival probability, the threshold field for the relaxation time up to microseconds or submicroseconds could be estimated, and an extrapolation was used to obtain the relaxation of 1 s, i.e., coersive field. Because the relaxation time increases very rapidly approaching the coercive field, the obtained coercive field is a good estimation.

Secondly, a coercivity estimation method using a magnetic field sweep in a practical simulation time was shown. In this method, the coercive field was obtained from the free energy barrier as a function of the field, which was estimated from the survival (unrelaxed) probability. This method worked well if the sweep range includes the stochastic relaxation region. Exact identification of the border between the initial transient and regular relaxation regions was not necessary, because the values of coercive field (field for zero-energy barrier as well) was not much affected by the fitting range. The consistency between the first and second estimation methods were confirmed. The second method has the advantage of being easier to handle. In addition, zero-field energy barrier and field for zero-energy barrier are obtained simultaneously with the coercive field.

The methodologies presented here can be applied to any types of metastable states, once the corresponding Hamiltonian is given. As mentioned in the introduction, the control of coercivity by nanoparticles of ferrites and molecular magnets is a hot topic. The application of the methods to these systems is our next target. Using our methods, the effect of the shell on the enhancement of the coercivity of core-shell nanoparticles of Prussian blue analogues can be estimated quantitatively, and the size dependence of the coercive field of nano particles of the epsilon iron can be studied in detail.

ACKNOWLEDGMENTS

The authors would like to thank Dr. Hirosawa for instructive discussions on experimental estimations of coercive fields. We also thank Dr. Hayasaka for useful discussions on coercivity estimation by theoretical approaches. This work was supported by World Premier International Research Center Initiative (WPI), MEXT, Japan and by Grants-in-Aid for Scientific Research B (No. 24K01332) from MEXT. Numerical calculations were performed using the Numerical Materials Simulator at the National Institute for Materials Science.

Appendix A: Hamiltonian for rare earth magnets

We adopt the following atomistic Hamiltonian for the Nd magnet. This Hamiltonian can be used for rare earth magnets, in which f electrons play an important role in magnetic properties.

$$\mathcal{H} = -\sum_{i<j} 2J_{ij}\boldsymbol{s}_i \cdot \boldsymbol{s}_j - \sum_{i}^{\mathrm{Fe}} D_i (s_i^z)^2 + \sum_{i}^{\mathrm{Nd}} \sum_{l,m} \Theta_{l,i} A_{l,i}^m \langle r^l \rangle_i \hat{O}_{l,i}^m - H \sum_i S_i^z. \tag{A1}$$

Here, J_{ij} is the exchange interaction between the ith and jth sites, and D_i is the magnetic anisotropy constant for Fe atoms. The third term is the crystal electric field (CEF) energy of Nd atoms. The origin of this term is the electrostatic interaction between f electrons of rare-earth atoms, and it is important for magnetic properties of rare-earth magnets. $\Theta_{l,i}$, $A_{l,i}^m$, $\langle r^l \rangle_i$, and $\hat{O}_{l,i}^m$ are the Stevens factor, coefficient of the spherical harmonics of the crystalline electric field, average of r^l over the radial wave function, and Stevens operator, respectively. We treat $l = 2, 4, 6$ and $m = 0$ (diagonal operators), which provide the dominant contribution. The fourth term is the Zeeman term, and H is the external magnetic field.

For Fe and B atoms, $\boldsymbol{s}_i$ denotes the magnetic moment at the ith site, while for Nd atoms, it is the moment of the

valence ($5d$ and $6s$) electrons. The total moment for Nd atoms at the ith site is $\boldsymbol{S}_i = \boldsymbol{s}_i + \boldsymbol{\mathcal{J}}_i$, where $\boldsymbol{\mathcal{J}}_i = g_{\rm T}\boldsymbol{J}_i\mu_{\rm B}$ with the magnitude of the total angular momentum, $J = 9/2$, and Landé g-factor, $g_{\rm T} = 8/11$. We define $\boldsymbol{S}_i = \boldsymbol{s}_i$ for Fe and B atoms. The details of the model are given in our previous papers [38, 39]. The magnetic interactions were mainly obtained from first-principles computation methods. The crystallographic information of $Nd_2Fe_{14}B$ and all the parameter values for the model (A1) were given in Ref. [39] and its supplemental material.

The simulated spin-reorientation transition temperature, $T_{\rm r} = 150$ K, was close to the experimentally estimated ones [20–22, 40]. The simulated critical temperature, $T_{\rm c} \sim 870\,{\rm K}$ was a little overestimated from the experimental values $T_{\rm c} \sim 600\,{\rm K}$ [17, 20], which is due to an overestimation of the exchange interactions. We are interested in room temperature properties and set $T = 400\,{\rm K} \simeq 0.46T_{\rm c}$, which is close to room temperature practically.

[1] P. Gütlich and H. A. Goodwin, eds., *Spin Crossover in Transition Metal Compounds I, II, III* (Springer, Berlin, 2004).

[2] M. A. Halcrow, ed., *Spin-crossover materials - properties and applications* (John Wiley & Sons, Chichester, UK, 2013).

[3] M. Verdaguer, A. Bleuzen, V. Marvaud, J. Vaissermann, M. Seuleiman, C. Desplanches, A. Scuiller, C. Train, R. Garde, G. Gelly, C. Lomenech, I. Rosenman, P. Veillet, C. Cartier, and F. Villain, Molecules to build solids: high Tc molecule-based magnets by design and recent revival of cyano complexes chemistry, Coordination Chemistry Reviews **190-192**, 1023 (1999).

[4] J. J. Zakrzewski, M. Liberka, J. Wang, S. Chorazy, and S. Ohkoshi, Optical phenomena in molecule-based magnetic materials, Chemical Reviews **124**, 5930 (2024).

[5] L. Catala, D. Brinzei, Y. Prado, A. Gloter, O. Stéphan, G. Rogez, and T. Mallah, Core-multishell magnetic coordination nanoparticles: Toward multifunctionality on the nanoscale, Angewandte Chemie International Edition **48**, 183 (2009).

[6] Y. Prado, S. Mazerat, E. Rivire, G. Rogez, A. Gloter, O. Stphan, L. Catala, and T. Mallah, Magnetization reversal in $CsNi^{II}Cr^{III}(CN)_6$ coordination nanoparticles: Unravelling surface anisotropy and dipolar interaction effects, Advanced Functional Materials **24**, 5402 (2014).

[7] S. Ohkoshi, S. Sakurai, J. Jin, and K. Hashimoto, The addition effects of alkaline earth ions in the chemical synthesis of ε-Fe_2O_3 nanocrystals that exhibit a huge coercive field, Journal of Applied Physics **97**, 10K312 (2005).

[8] A. Namai, M. Yoshikiyo, K. Yamada, S. Sakurai, T. Goto, T. Yoshida, T. Miyazaki, M. Nakajima, T. Suemoto, H. Tokoro, and S. Ohkoshi, Hard magnetic ferrite with a gigantic coercivity and high frequency millimetre wave rotation, Nature Communications **3**, 1035 (2012).

[9] S. Miyashita, *Collapse of Metastability* (Springer-Nature, 2022).

[10] H. Kronmüller and M. Fähnle, *Micromagnetism and the Microstructure of Ferromagnetic Solids*, Cambridge studies in magnetism (Cambridge University Press, 2003).

[11] H. Hayasaka, M. Nishino, and S. Miyashita, Microscopic study on the angular dependence of coercivity at zero and finite temperatures, Phys. Rev. B **105**, 224414 (2022).

[12] M. Nishino, I. E. Uysal, T. Hinokihara, and S. Miyashita, Dynamical aspects of magnetization reversal in the neodymium permanent magnet by a stochastic Landau-Lifshitz-Gilbert simulation at finite temperature: Real-time dynamics and quantitative estimation of coercive force, Phys. Rev. B **102**, 020413(R) (2020).

[13] M. Nishino and S. Miyashita, Quantitative estimation of coercive field in a ferromagnetic grain using field sweep simulation, Phys. Rev. B **107**, 184422 (2023).

[14] M. Sagawa and S. Hirosawa, Magnetic hardening mechanism in sintered *R*–Fe–B permanent magnets, Journal of Materials Research **3**, 45 (1988).

[15] J. F. Herbst, J. J. Croat, F. E. Pinkerton, and W. B. Yelon, Relationships between crystal structure and magnetic properties in $Nd_2Fe_{14}B$, Phys. Rev. B **29**, 4176 (1984).

[16] S. Hirosawa, Y. Matsuura, H. Yamamoto, S. Fujimura, M. Sagawa, and H. Yamauchi, Single crystal measurements of anisotropy constants of $R_2Fe_{14}B$ (R=Y, Ce, Pr, Nd, Gd, Tb, Dy and Ho), Japanese Journal of Applied Physics **24**, L803 (1985).

[17] A. V. Andreev, A. V. Deriagin, N. V. Kudrevatykh, N. V. Mushnikov, and V. A. Reimer, The magnetism of $Y_2Fe_{14}B$ and $Nd_2Fe_{14}B$ and their hydrides, Zhurnal Eksperimentalnoi i Teoreticheskoi Fiziki **90**, 1042 (1986).

[18] H. Kronmller, K.-D. Durst, and M. Sagawa, Analysis of the magnetic hardening mechanism in RE-FeB permanent magnets, Journal of Magnetism and Magnetic Materials **74**, 291 (1988).

[19] J. F. Herbst, $R_2Fe_{14}B$ materials: Intrinsic properties and technological aspects, Rev. Mod. Phys. **63**, 819 (1991).

[20] S. Hirosawa, Y. Matsuura, H. Yamamoto, S. Fujimura, M. Sagawa, and H. Yamauchi, Magnetization and magnetic anisotropy of $R_2Fe_{14}B$ measured on single crystals, Journal of Applied Physics **59**, 873 (1986).

[21] O. Yamada, Y. Ohtsu, F. Ono, M. Sagawa, and S. Hirosawa, Magnetocrystalline anisotropy in $Nd_2Fe_{14}B$ intermetallic compound, Journal of Magnetism and Magnetic Materials **70**, 322 (1987).

[22] N. V. Mushnikov, P. B. Terent'ev, and E. V. Rosenfel'd, Magnetic anisotropy of the $Nd_2Fe_{14}B$ compound and its hydride $Nd_2Fe_{14}BH_4$, The Physics of Metals and Metallography **103**, 39 (2007).

[23] T. Kohashi, K. Motai, T. Nishiuchi, and S. Hirosawa, Magnetism in grain-boundary phase of a NdFeB sintered magnet studied by spin-polarized scanning electron microscopy, Applied Physics Letters **104**, 232408 (2014).

[24] S. Hirosawa, M. Nishino, and S. Miyashita, Perspectives for high-performance permanent magnets: applications, coercivity, and new materials, Advances in Natural Sciences: Nanoscience and Nanotechnology **8**, 013002 (2017).

[25] Y. Toga, S. Miyashita, A. Sakuma, and T. Miyake, Role of atomic-scale thermal fluctuations in the coercivity, npj Computational Materials **6**, 67 (2020).

[26] F. Wang and D. P. Landau, Efficient, multiple-range random walk algorithm to calculate the density of states, Phys. Rev. Lett. **86**, 2050 (2001).

[27] S. Mohakud, S. Andraus, M. Nishino, A. Sakuma, and S. Miyashita, Temperature dependence of the threshold magnetic field for nucleation and domain wall propagation in an inhomogeneous structure with grain boundary, Phys. Rev. B **94**, 054430 (2016).

[28] J. L. García-Palacios and F. J. Lázaro, Langevin-dynamics study of the dynamical properties of small magnetic particles, Phys. Rev. B **58**, 14937 (1998).

[29] M. Nishino and S. Miyashita, Realization of the thermal equilibrium in inhomogeneous magnetic systems by the Landau-Lifshitz-Gilbert equation with stochastic noise, and its dynamical aspects, Phys. Rev. B **91**, 134411 (2015).

[30] D. Givord, A. Lienard, P. Tenaud, and T. Viadieu, Magnetic viscosity in Nd-Fe-B sintered magnets, Journal of Magnetism and Magnetic Materials **67**, L281 (1987).

[31] W. Wernsdorfer, E. B. Orozco, K. Hasselbach, A. Benoit, B. Barbara, N. Demoncy, A. Loiseau, H. Pascard, and D. Mailly, Experimental evidence of the Néel-Brown model of magnetization reversal, Phys. Rev. Lett. **78**, 1791 (1997).

[32] S. Okamoto, R. Goto, N. Kikuchi, O. Kitakami, T. Akiya, H. Sepehri-Amin, T. Ohkubo, K. Hono, K. Hioki, and A. Hattori, Temperature-dependent magnetization reversal process and coercivity mechanism in Nd-Fe-B hot-deformed magnets, Journal of Applied Physics **118**, 223903 (2015).

[33] S. Okamoto, Experimental approaches for micromagnetic coercivity analysis of advanced permanent magnet materials, Science and Technology of Advanced Materials **22**, 124 (2021).

[34] D. Givord, P. Tenaud, and T. Viadieu, Coercivity mechanisms in ferrites and rare earth transition metal sintered magnets ($SmCo_5$, Nd-Fe-B), IEEE Transactions on Magnetics **24**, 1921 (1988).

[35] P. Gaunt, Magnetic viscosity and thermal activation energy, Journal of Applied Physics **59**, 4129 (1986).

[36] T. Pokhil and E. Nikolaev, Domain wall motion in Re-Tm films with different thickness, IEEE Transactions on Magnetics **29**, 2536 (1993).

[37] K.-J. Kim, J. Ryu, G.-H. Gim, J.-C. Lee, K.-H. Shin, H.-W. Lee, and S.-B. Choe, Electric current effect on the energy barrier of magnetic domain wall depinning: Origin of the quadratic contribution, Phys. Rev. Lett. **107**, 217205 (2011).

[38] M. Nishino, Y. Toga, S. Miyashita, H. Akai, A. Sakuma, and S. Hirosawa, Atomistic-model study of temperature-dependent domain walls in the neodymium permanent magnet $Nd_2Fe_{14}B$, Phys. Rev. B **95**, 094429 (2017).

[39] S. Miyashita, M. Nishino, Y. Toga, T. Hinokihara, I. E. Uysal, T. Miyake, H. Akai, S. Hirosawa, and A. Sakuma, Atomistic theory of thermally activated magnetization processes in $Nd_2Fe_{14}B$ permanent magnet, Science and Technology of Advanced Materials **22**, 658 (2021).

[40] M. Yamada, H. Kato, H. Yamamoto, and Y. Nakagawa, Crystal-field analysis of the magnetization process in a series of $Nd_2Fe_{14}B$-type compounds, Phys. Rev. B **38**, 620 (1988).

Graphical abstract

We developed methods for quantitatively estimating the relaxation time of a long-lived metastable magnetic state, as well as the coercive field. These methods overcome the difficulties of limited simulation time and treat the broad distribution of relaxation times arising from stochastic processes.